MODELING OF SLANT AND CUP-CONE FRACTURE OF METALS

W. BROCKS[1], J. BESSON[2] AND D. STEGLICH[1]

[1)] *GKSS Research Centre*
D-21502 Geesthacht, Germany
[2)] *Centre des Materiaux,*
Ecole des Mines de Paris, France

ABSTRACT

The formation of slant and cup-cone fracture under plane strain and axisymmetric conditions, respectively, is studied using the finite element (FE) method. Constitutive models for ductile damage proposed by Rousselier and by Gurson are applied. The respective equations allowing for finite strain were implemented in two FE codes, ABAQUS and Zébulon. The ability of both models to represent cup-cone fracture of round bars and shear fracture of plane strain specimens, in general, and influences of material parameters and mesh design, in particular, are studied. Material data of three different materials are used: a high purity modern steel, an aluminum alloy (2024 series) and a cast iron containing spherical graphite inclusions. These materials allow to study a wide range of initial void volume fractions, f_0, and different hardening behaviours. Two test sample geometries were selected: (i) smooth round bars, (ii) plane strain ("Hill") specimens.

KEYWORDS

ductile damage, numerical simulation, localization, Gurson model, Rousselier model

INTRODUCTION

Constitutive models for describing damage evolution in ductile materials have found increasing application, mainly the micromechanical GTN model by Gurson [1], Tvergaard and Needleman [2-4], and a continuum damage mechanics approach by Rousselier [5]. They are based on the physical understanding that in the course of plastic deformation microvoids nucleate and grow until a localized plastic necking or fracture of the intervoid matrix occurs. Both models modify the von Mises yield potential by introducing a single scalar damage quantity, namely the void volume fraction, f.

These models have been successfully applied to model crack propagation in precracked structures (Needleman and Tvergaard [6], Sun et al. [7], Brocks et al. [8], Xia et al. [9]). But also ductile rupture of uncracked laboratory specimens such as smooth and notched round tensile bars (Tvergaard and Needleman [3, 4], Becker et al. [10]) or plane strain specimens (Becker and Needleman [11], Leblond et al. [12]) has been numerically simulated. Fracture of these specimens involves both, initiation and propagation of a crack. Phenomena like "cup-cone" fracture in round bars and "slant" fracture in plane strain specimens are observed experimentally, see Fig. 1, where localization of damage and deformation is not perpendicular to the principle loading direction. The present paper studies the abilities of the Gurson and the Rousselier model to simulate these phenomena by the finite element method and investigates the influences of mesh design and material parameters.

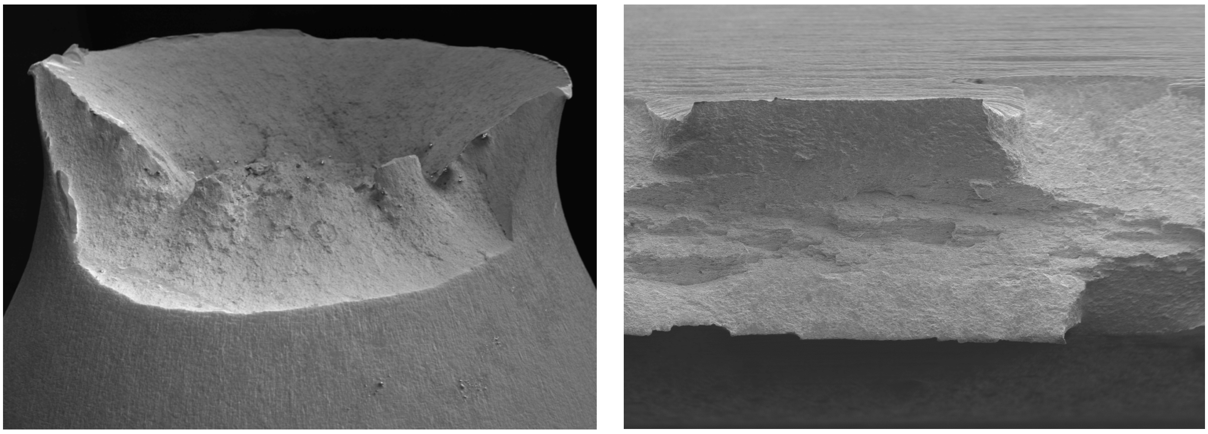

Fig. 1. Cup-cone fracture in a round tensile bar (left) and slant fracture in a Hill specimen (right)

The condition for localization, that means the possibility of forming a strain rate discontinuity in elasto-plastic solids has been established by Rice [13], and the case of dilatant pressure sensitive materials has been investigated by Rudnicki and Rice [14]. The susceptibility of the Gurson model to localization was first studied by Yamamoto [15], and this model has been used by Tvergaard [16] to investigate the evolution of shear bands. The role of kinematic hardening was investigated by Mear and Hutchinson [17] and, together with void nucleation, by Tvergaard [18]. However, all these analyses are limited to the idealized situation of an infinite medium in which a discontinuity band appears. For real structures, Doghri and Billardon [19] proposed to compute Rice's condition for localization during the FE calculation. Following this idea, a localization indicator has been evaluated and the computed crack path has been compared with the prediction obtained from this indicator.

SIMULATION OF DUCTILE DAMAGE AND FRACTURE

Damage models of Gurson and Rousselier

Ductile tearing of metals is dominated by the mechanisms of void nucleation at particles, void growth and coalescence by necking of the intervoid matrx. The inelastic deformation is described by a modified yield function and plastic potential, Φ, including the "porosity" in terms of the void volume fraction, f, as an additional internal variable which is responsible for the "softening" of the material. The most common constitutive model for describing this process was derived by Gurson [1] based on a micromechanical consideration of a spherical and a cylindrical hole in an elasto-plastic matrix. The stress and strain fields in this representative micro-cell are averaged over its volume by

$$\begin{aligned}\overline{\mathbf{T}} &= \frac{1}{V}\int_V \mathbf{T}(\mathbf{x})\,d\tilde{V} = \frac{1}{V}\int_{\partial V} \mathbf{x}\,\mathbf{t}\,d\tilde{A}\,,\\ \overline{\mathbf{E}} &= \frac{1}{V}\int_V \tfrac{1}{2}\left[\nabla\mathbf{u} + \mathbf{u}\nabla\right]d\tilde{V} = \frac{1}{V}\int_{\partial V} \tfrac{1}{2}\left(\mathbf{n}\,\mathbf{u} + \mathbf{u}\,\mathbf{n}\right)d\tilde{A}\,,\end{aligned} \tag{2}$$

and an approximate yield function is obtained on a "meso-scale". Gurson's yield potential was later modified by Tvergaard and Needleman [2-4], giving it the final form

$$\varPhi = \frac{3\overline{\mathbf{T}}' \cdot\cdot \overline{\mathbf{T}}'}{2\sigma_{\mathrm{Y}}^2} + 2q_1 f^* \cosh\left(q_2 \frac{\mathrm{tr}\,\overline{\mathbf{T}}}{2\sigma_{\mathrm{Y}}} \right) - \left(1 + q_3 f^{*2}\right), \tag{1}$$

which is adressed as GTN model. $\overline{\mathbf{T}}$ is the "mesoscopic" Cauchy stress tensor and $\overline{\mathbf{T}}'$ its deviator, $\sigma_{\mathrm{Y}}\left(\varepsilon^p\right)$ is the yield stress of the matrix material, and q_i (i = 1, 2, 3), are phenomenological parameters introduced by Tvergaaard and Needleman. Commonly, they are taken as $q_1 = 1.5$, $q_2 = 1.0$, $q_3 = q_1^2 = 2.25$, which is also adopted here with some exceptions concerning q_2 which will be indicated later. The yield condition incorporates the effects of the hydrostatic stress, $\sigma_{\mathrm{h}} = \mathrm{tr}\mathbf{T}$, and the respective effect is scaled by q_2. "Porous" materials are pressure sensitive and the inelastic deformation is not isochoric.

An alternative formulation of the plastic potential also introducing a scalar variable of porosity has been propsed by Rousselier [5]. It is based on the concept of continuum damage mechanics that the "effective stress" in a damaged continuum is given by $\hat{\mathbf{T}} = \mathbf{T}/(1-f)$. Together with some considerations on thermodynamic potentials he obtained

$$\varPhi = \frac{\sqrt{\frac{3}{2}\mathbf{T}' \cdot\cdot \mathbf{T}'}}{(1-f)\sigma_{\mathrm{Y}}} + \frac{\sigma_1}{\sigma_{\mathrm{Y}}} f\, D \exp\left(\frac{\mathrm{tr}\mathbf{T}}{3(1-f)\sigma_1} \right) - 1. \tag{3}$$

Here, D and σ_1 are material parameters. While the actual porosity f is used as an internal variable in Rousselier´s yield function, f^* in Tvergaaard's and Needleman's modification of Gurson's plastic potential represents an "effective" porosity,

$$f^* = \begin{cases} f & \text{for} \quad f \le f_c \\ f_c + \dfrac{f_u^* - f_c}{f_f - f_c}(f - f_c) & \text{for} \quad f > f_c \quad \text{with} \quad f_u^* = \dfrac{1}{q_1} \end{cases}, \tag{4}$$

which is supposed to describe the whole range from void growth to coalescence up to final fracture by introducing two additional parameters, namely f_{c} and f_{f}.

In both models, the plastic deformation rate, $\mathbf{D}^{\mathrm{p}}$, is obtained assuming the normality rule of plasticity, and the evolution of porosity is given by mass conservation,

$$\dot{f} = (1-f)\mathrm{tr}\mathbf{D}^{\mathrm{p}} \quad \text{with} \quad f(t_0) = f_0 . \tag{5}$$

f_0 is the initial void volume fraction. This equation may be modified in both models to account for nucleation of voids by adding a second term, f_{nuc}. For strain controlled nucleation, this term is given by

$$\dot{f}_{\mathrm{nuc}} = A_{\mathrm{n}} \dot{\varepsilon}^p . \tag{6}$$

A phenomenological model of nucleation proposed by Chu and Needleman [20] involves three additional parameters, the ratio of void nucleating parameters, f_{n}, the average nucleation strain, ε_n, and the standard deviation of nucleation strains, s_n. A simplified nucleation term has been used in the present investigation, assuming that nucleation starts for $f > f_c$ and A_n is constant (Besson et al. [21, 22]).

Although both models of porous metal plasticity are essentially similar two important differences have to be outlined, see Fig. 2:

1. Under pure shear loading, i.e. $\sigma_h = 0$, the Rousselier model predicts void growth, $\dot{f} > 0$, whereas the Gurson model does not.
2. Under pure hydrostatic loading, i.e. $\sigma_e = 0$, the Rousselier yield surface has a vertex which implies that, different from the Gurson model, even at high triaxiality ratios the plastic deformation tensor always keeps a non-zero shear component.

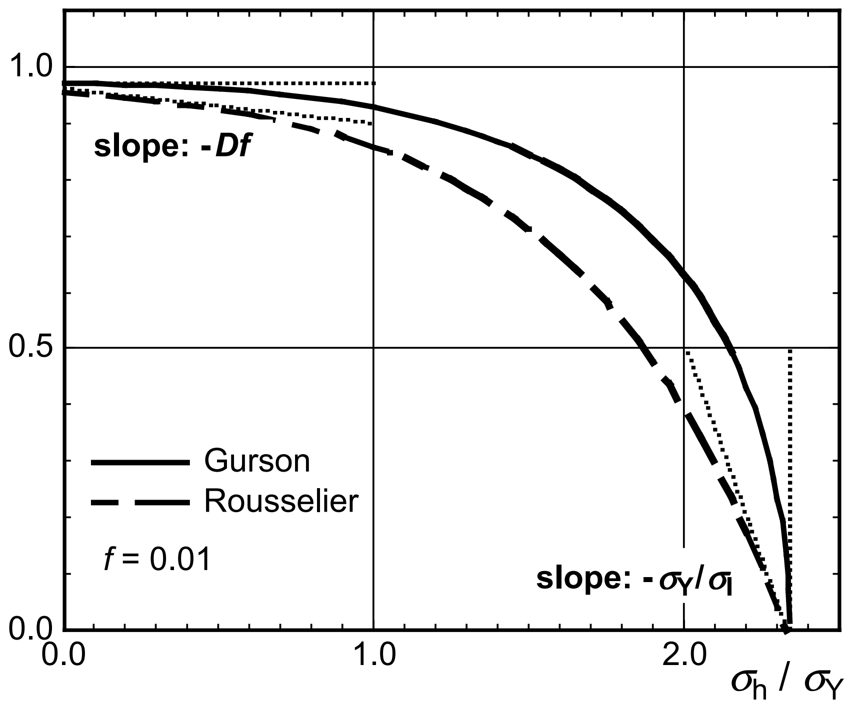

Fig. 2. Comparison of the Gurson and Rousselier yield surfaces; respective parameters calibrated to give the same results for both models under pure shear and pure hydrostatic stress.

Both Gurson and Rousselier model have been implemented in the FE codes ABAQUS, following the method of Aravas [22], and Zébulon (Foerch et al. [23], Besson et al. [25]). A fully implicit time integration scheme is used (Zhang [26]). Finite strains were treated using co-rotational reference frames with Jaumann stress rate (Hughes and Winget [27]).

Localization indicator

Localization of strain and damage was first analyzed by Rice [13] for an elasto-plastic material in which a planar band of strain rate discontinuity forms. This band is characterized by its unit normal, **n**, and the displacement jump across the band whose orientation is denoted by the unit vector **g**. In the case of porous materials, **g** and **n** are not necessarily orthogonal. The strain rate tensor across the discontinuity band can be expressed as (Rice and Rudnicki [28])

$$\mathbf{D} = \tfrac{1}{2}(\mathbf{gn} + \mathbf{ng}). \tag{7}$$

Bifurcation is given by the condition that the second order "acoustic" tensor, $\mathbf{A} = \mathbf{n} \cdot \underline{\mathbf{L}} \cdot \mathbf{n}$, has a zero eigenvalue,

$$\exists \mathbf{n}: \quad \det(\mathbf{n} \cdot \underline{\mathbf{L}} \cdot \mathbf{n}) = 0\,, \tag{8}$$

where $\underline{\mathbf{L}}$ is the fourth order elasto-plastic tangent matrix within the incremental constitutive equation $\overset{\nabla}{\mathbf{T}} = \underline{\mathbf{L}} : \mathbf{D}$. The localization indicator,

$$I_{\mathrm{loc}} = \min_{\mathbf{n}} \left[\det(\mathbf{n} \cdot \underline{\mathbf{L}} \cdot \mathbf{n})\right], \tag{9}$$

was implemented in the FE calculations to monitor the possibility of bifurcation at any material point. As $\det(\mathbf{n} \cdot \underline{\mathbf{L}} \cdot \mathbf{n}) = 0$ will never be met exactly, localization will be defined as occuring when $I_{\mathrm{loc}} < 0$ for the first time. For further details of the localization analysis see Besson et al. [22].

Material parameters and specimens

Material data of three different materials are used:

- a high strength low alloyed ferritic-perlitic steel, X70 HSLA (Rivalin [29]),
- a 2024 aluminum alloy (Besson et al. [21]), and
- a cast iron containing spherical graphite inclusions, GGG40 (Steglich [30]).

These materials allow to study a wide range of initial void volume fractions, f_0, and different hardening behaviours. The material parameters for elasto-plastic deformation and damage were fitted to test data of smooth and notched bars. The parameters of the damage models are summarized in Table 1. The q-parameters are taken as $q_1 = 1.5$ and $q_3 = q_1^2 = 2.25$, whereas q_2 which scales the influence of stress triaxiality varies and is specified in the table. Different parameter sets of the Gurson model, denoted by G, G* and G_n, respectively, were used for the steel, which will be discussed below.

Table 1. Parameters of the Gurson and the Rousselier model for the three investigated materials

material	steel X70 HSLA			Al 2024 A	GGG40
Gurson model	G	G*	G_n		
f_0	0.00015	0.00015	0.00015	0.0012	0.12
f_c	-	0.005	0.005	0.018	0.175
f_f	-	0.225	-	0.18	0.235
A_n	-	-	0.2	-	-
q_2	1.15	1.0	1.0	2.0	1.0
Rousselier model					
D	1.4			2.0	-
σ_1 [MPa]	451			260	-

Two test sample geometries were selected which allow for two-dimensional calculations:

- a smooth round bar and
- a plane strain or "Hill" specimens, see Fig. 3.

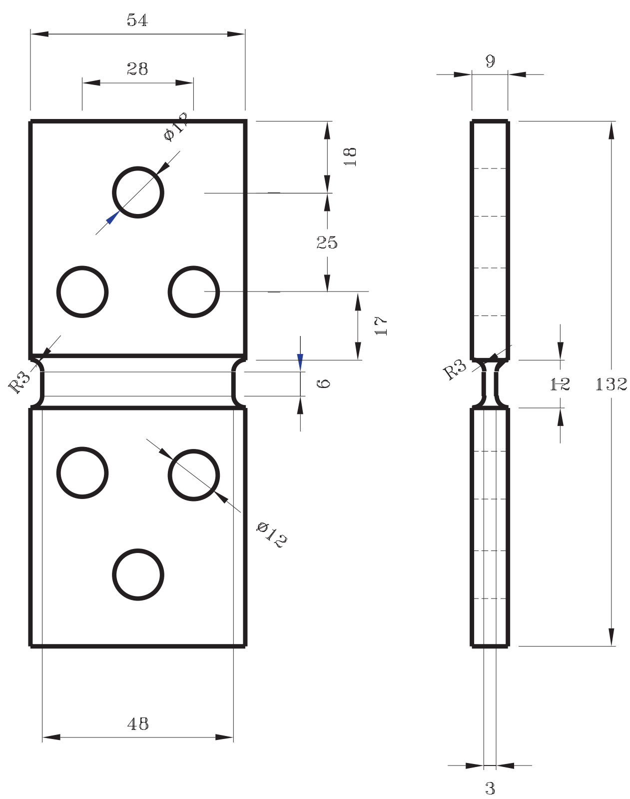

Fig. 3. Hill specimen: plane strain condition is reached in the centre strip

RESULTS

Finite element simulations were performed using the FE codes ABAQUS and Zébulon. All calculations except the studies on the effect of element type were performed using quadratic (8 nodes) axisymmetric or plane strain elements with reduced integration (4 Gauss points). As very similar results in terms of mesh dependence, occurence of localization and slant or cup-cone fracture were obtained with both FE codes only some examples using one or the other will be presented in the following. Results of the steel X70 HSLA are presented if not indicated otherwise. No artificial imperfections meshes to promote localization have been applied to the FE.

Mesh size and mesh design
Mesh size and mesh design play an important role in numerical simulations of damage and fracture (Tvergaard and Needleman [3], Ruggieri et al. [31]). The element height determines the energy release rate (Xia et al. [9], Siegmund and Brocks [32]) and has to be adjusted to fit experimental crack growth resistance data (Rousselier [5], Sun and Hönig [33], Brocks and Steglich [34], Gullerud et al. [35). But beside the well known influence of the element height a number of additional effects on the crack formation have been found, namely any imposed symmetry of the mesh, the number of elements across the specimen section and the element type. Little attention has been given to the latter though unit cell calculations by Brocks et al. [36] have revealed a significant influence of the element type on the plastic collapse which is the structural equivalence to void coalescence and determines the f_c value in the GTN model.

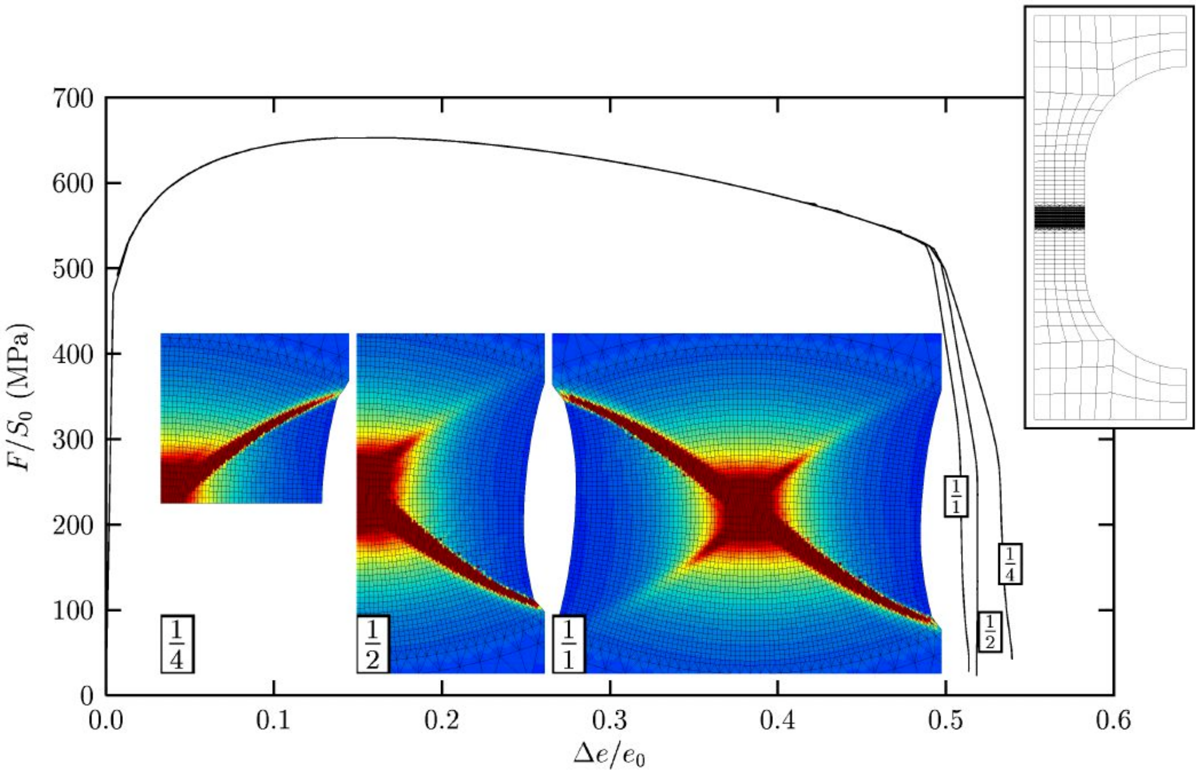

Fig. 4. Mesh symmetry effect on load vs displacement curve and crack formation: Rousselier model, FE-code Zébulon, quarter, half and full plane strain specimen, number of elements over half specimen thickness 40, element aspect ratio 3.25; contours show damage at final rupture; S_0 = initial cross section, e_0 = initial thickness.

Mesh symmetry effect. Taking full advantage of symmetries of the round bar or the Hill specimen requires meshing of one quarter, only, which is usually adopted to reduce the number of degrees of freedom in the FE model. However, meshing of one quarter of the specimen means that in the case of slant fracture two cracks forming a cross or in the case of cup-cone fracture (Tvergaard and Needleman [3]) two cones are actually modelled. This leeds to a higher value of dissipated energy. Fig. 4 shows the load vs reduction of thickness curves and the crack formation obtained from simulations of one quarter, one half and full specimen models. Failure is delayed in the case of the quarter model. The effect of imposed symmetry becomes relevant at the sudden drop of the load, i.e. when a crack initiates in the centre of the specimen.

Element size effect. The number of elements over the specimen cross section does not significantly affect the load displacement curve until significant damage occurs and a micro-crack has initiated in the specimen, which is indicated by the sudden drop of the load in the final stage. Increasing the number of elements in the cross section of the specimen causes the crack to grow faster and the load drop to become steeper, see Fig. 5. This is an effect of the element height because this dimension is proportional to the dissipated energy per crack growth increment (Ruggieri et al. [31]). But as the aspect ratio has been kept constant (width : height = 3.25 : 1) in these calculations, increasing number of elements means also decreasing height. The number of elements affects the formation of the crack surface: a minimum number is required to obtain slant (or cup-cone) fracture, see Fig. 6. As the continuum mechanics description does not involve any length scale, this is definitely a question of the number of elements and not of their absolute size.

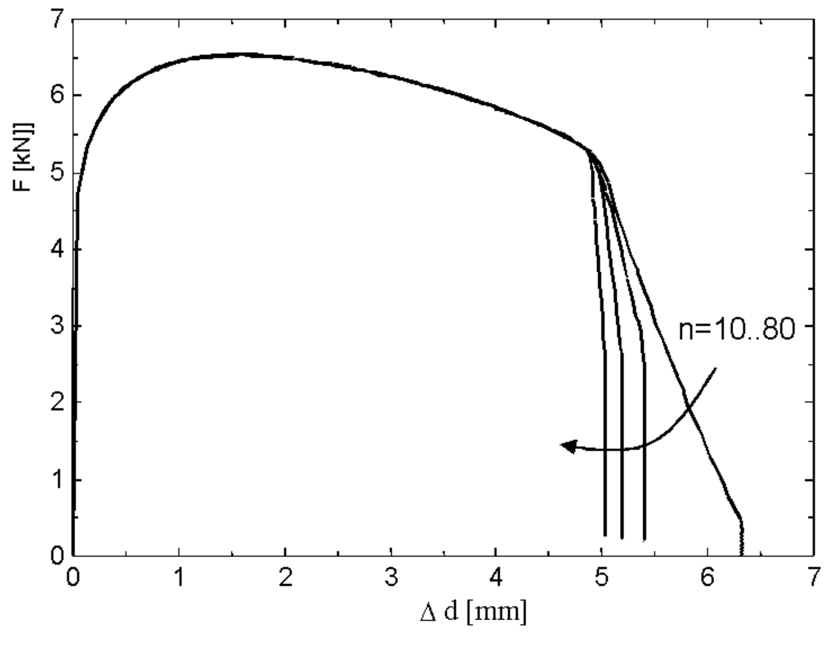

Fig. 5. Element size effect on load vs reduction of thickness: Rousselier model, FE-code Zébulon, plane strain specimen, number of elements over half specimen thickness 10, 20, 40, 80, element aspect ratio 3.25 : 1.

Effect of element aspect ratio. The element height is proportional to the dissipated energy during the fracture process whereas the element width is important to reproduce the gradients of stress and strain fields adequately. For a given number of elements, i.e. fixed element width, the element aspect ratio appeared to be of minor influence for the formation of slant fracture in the plane strain specimen (Besson et al. [22]) but affects the rupture mode, cup-cone or flat fracture, of round bars. Fig. 6 displays a matrix of the effects of element widths and aspect ratios.

number of elements aspect ratio	20	40	80
12 : 1	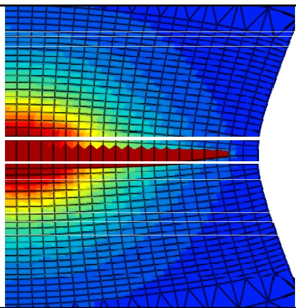	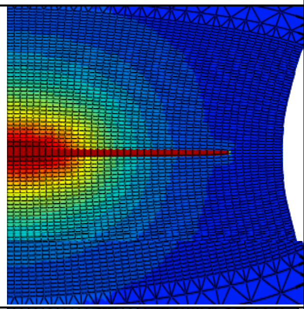	
6: 1	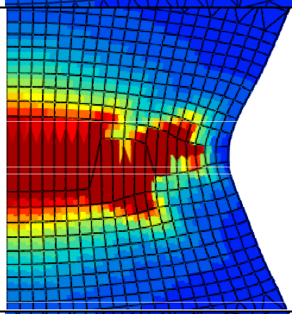	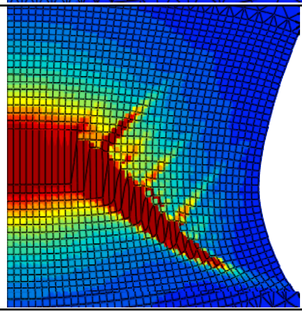	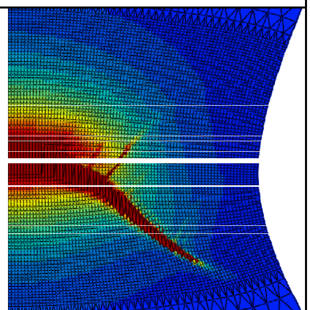
3 : 1	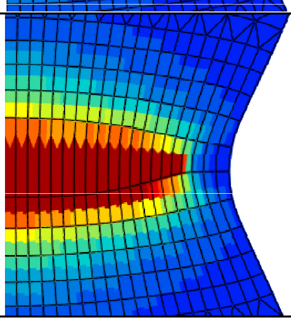	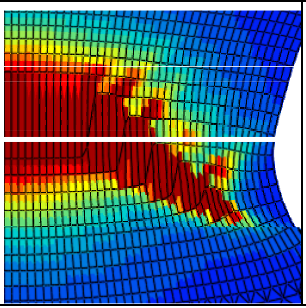	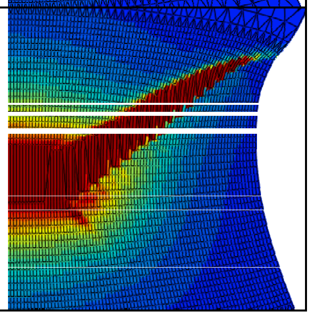

Fig. 6. Effect of number of elements and element aspect ratio (width : height) on fracture surface formation: Rousselier model, FE-code Zébulon, round bar; contours show damage at final rupture.

Effect of element type. Applying linear (4 nodes) or quadratic (8 nodes) quadrilateral or triangular elements affects the formation of cup-cone or flat fracture, see Fig. 7. Triangular elements obviously promote deviation of the crack. Note, that Needleman and Tvergaard [4] used quadrilaterals which were sub-divided onti four triangles in their investigation on cup-cone fracture. The two simulations with linear elements displayed in the bottom row of Fig. 7 differ by the number of elements, namely 40 and 80, over the thickness. Again, a minimum number of elements is required to obtain cup-cone fracture.

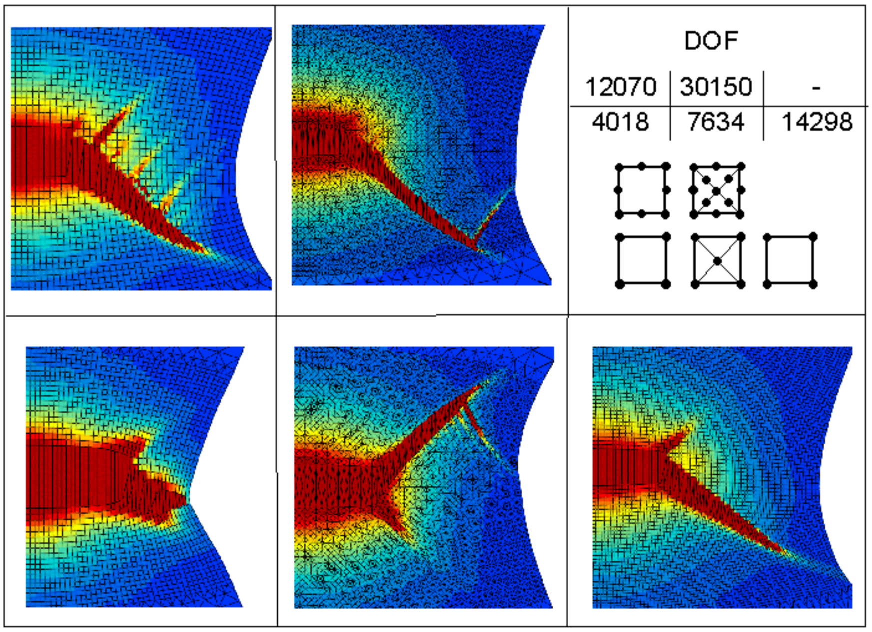

Fig. 7. Effect of element formulation on fracture surface formation: Rousselier model, FE-code Zébulon, round bar; contours show damage at final rupture.

Formation of fracture surfaces by the Gurson and the Rousselier model.
All the previous examples showed simulations with the Rousselier model. In general, slant or cup-cone fracture is more easily obtained with the Rousselier than with the Gurson model, which is due to the differences in the yield surfaces pointed out in Fig. 2: under shear loading the Rousselier model predicts void growth whereas the Gurson model does not. Studying the characteristics of the GTN model with respect to slant or cup-cone fracture is much more complex, however, as it has a higher number of adjustable parameters which influence the results. Three variants have been studied, namely

- Gurson's original yield function without nucleation and without the modified damage function f^*, denoted by G
- the modified version by Tvergaard and Needleman with accelerated damage by introducing f^* according to eq. (4), denoted by G*, and
- the modified version additionally accounting for void nucleation if $f > f_c$ according to eq. (6), denoted by G_n.

The respective parameter sets are summarized in Table 1. The crack paths obtained in the FE simulations are compared in Fig. 8. All models except G* predict slant fracture. Similar results were obtained for cup-cone fracture of round bars. This result is somehow intriguing as most of the simulations in the literature apply the GTN model with the f^*-function of eq. (4). The localization indicator of eq. (7) was used by Besson et al. [22] to interpret this effect; just one example is presented below.

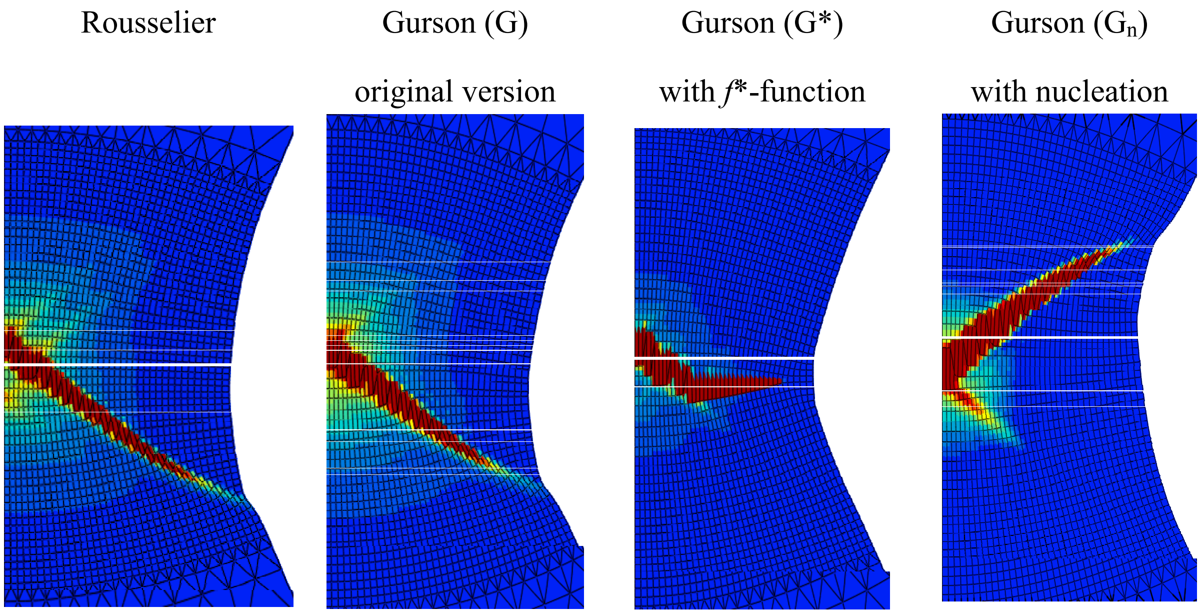

Fig. 8. Formation of crack surfaces by Rousselier's and Gurson's model: FE-code Zébulon, plane strain specimen, number of elements over half specimen thickness 40, element aspect ratio 3.5 : 1; contours show damage at final rupture.

The localization indicator, eq. (7), was implemented in the FE calculations to monitor the bifurcation condition in any material point. Localization is defined as occuring when $I_{loc} < 0$ for the first time. Fig 9 shows the evolution of this quantity (top row) and of the porosity (bottom row) in the necking section of the specimen for six successive load steps shortly before and after failure indicated by the sudden drop of the applied load, as predicted by the Rousselier model. The value of I_{loc} indicates three states,

- green (light grey): plastic deformation, $I_{loc} > 0$,
- yellow (medium grey): possible localization, $I_{loc} \leq 0$.
- blue (dark grey): elastic unloading.

Highly damaged areas, i.e. high values of f, are indicated in red (black).

Localization indicator and porosity evolve as follows:

(1) Plastic necking of the cross section has proceeded and slightly increased porosity is observed in the centre.

(2) A small circular area of possible localization spreads from the centre, damage in the centre has further increased but still, no crack has initiated.

(3) Load starts to drop suddenly beyond this point. The area of possible localization has developed a kidney (or butterfly wing) shape, and a crack has initiated in the centre. Regions of elastic unloading are visible above and below the crack.

(4) Load further decreases, the crack starting from the centre starts bifurcating into ±45° directions, but the area of possible localization has reduced to a narrow band in -45° orientation. The regions of elastic unloading have increased.

(5) A principle crack has developed in the -45° orientation as indicated before by I_{loc}. The band of possible localization approaches the specimen surface.

(6) The load is close to zero and the principle crack has nearly reached the specimen surface. The major part of the specimen is elastically unloaded.

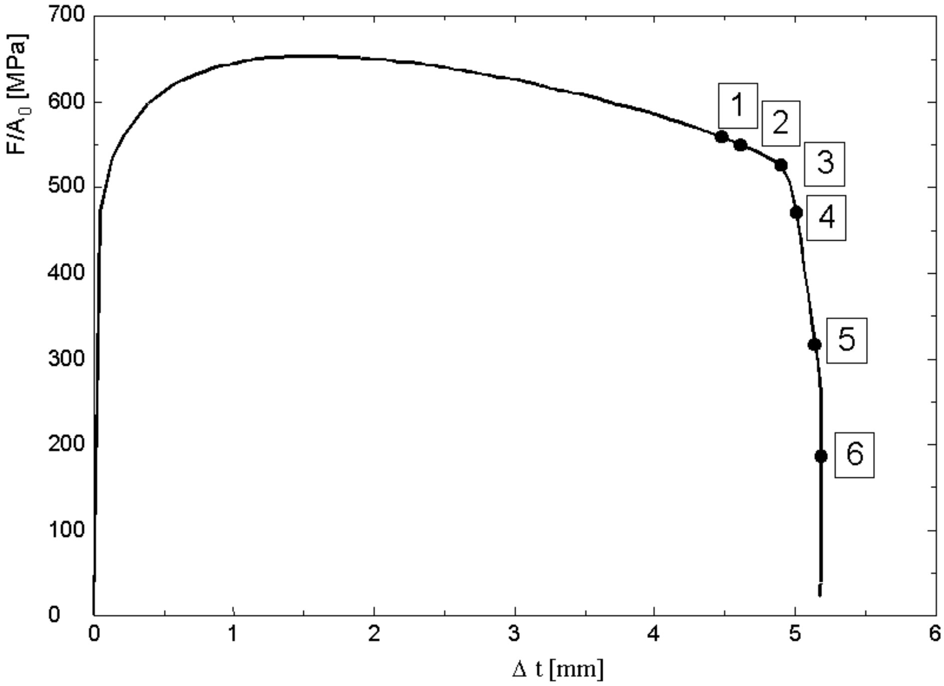

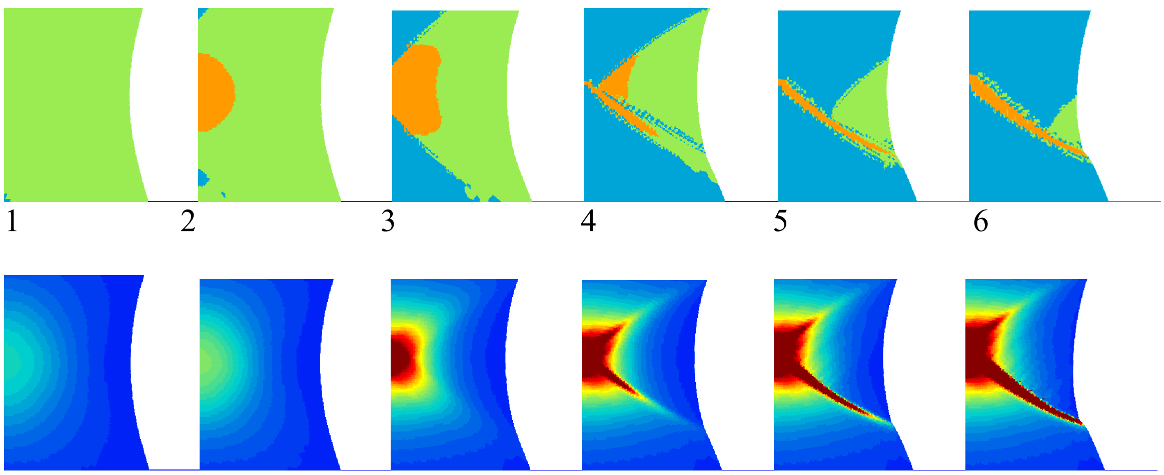

Fig. 9. Load vs reduction of thickness diagramme (A_0 = initial cross section, Δt = reduction of thickness) and evolution of the localization indicator (top row) and damage (bottom row) for six successive load steps shortly before and after failure: Rousselier model, FE-code Zébulon, plane strain specimen, number of elements over half specimen thickness 40, element aspect ratio 3.5 : 1.

The G-model gives essentially similar results to the Rousselier model. An elongated zone of possible localization, $I_{loc} \leq 0$, exists ahead of the slanted crack in which the crack will further propagate. In the case of the G*-model, however, this localization zone is much smaller and eventually disappears. This is due to the sharp bend in the f^*-function at f_c, eq. (6), which causes a spatial discontinuity of the localization indicator: localization may be possible at a single Gauss point whereas the surrounding Gauss points remain in a state far from instability. This inhibits the deviation of the crack from the flat fracture surface.

Influence of material properties

A systematic study of all possible effects of the various material parameters on the fracture surface formation is practically impossible. The three materials investigated in the present study, see Table 1, differed mainly by their initial void volume fraction, f_0, that means by their inclusion size and spacing. The matrix displayed in Fig. 10 gives some indication to the trends which can be expected without claiming generality. Initial porosity increases from the bottom to the top row. No cup-cone fracture could be obtained with the GTN model (in its conventionally used version including f^*) for any of the materials and no slant fracture for the low porosity steel. Rousselier model predicted cup-cone or slant fracture, respectively, for any of the materials, provided a sufficient number of elements over the specimen thickness, of course. Gurson and Rousselier model differ by the predicted inclination angle of the slant crack (Besson et al. [25])

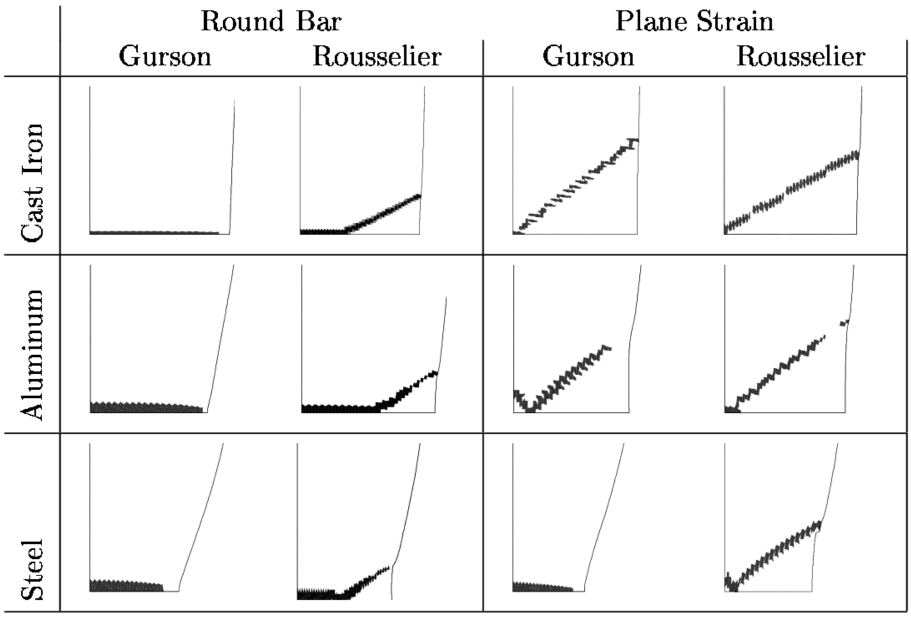

Fig. 10. Formation of the fracture surface in round bars and plane strain specimens for materials with different initial void volume fraction, f_0, as predicted by the Gurson and the Rousselier model.

CONCLUSIONS

The formation of slant and cup-cone fracture in numerical simulations using the Gurson and the Rousselier model has been analyzed. A localization idicator has been computed to detect zones of possible localization of deformation and damage.

In order to model slant or cup-cone fracture, a minimum number of elements must be used to discretize the cross section of the specimen. It was found that at least 15 elements over the half thickness are required for both models. Below this limit the mesh is to coarse to capture the localization zone. Other mesh design dependences are related to enforced symmetry conditions, the element aspect ratio and the element formulation.

Slant or cup-cone fracture is generally more easily obtained with the Rousselier than with the Gurson model, which is due to the differences in the respective yield surfaces. Applying the f^*-function in the GTN may inhibit slant fractureas the localization zone cannot extend sufficiently so that the crack surface remains flat. Slanted fracture can also be obtained with the void nucleation option. Similar conclusions were drawn from the study of cup-cone fracture by Besson et al. [25].

The inclination angle of the crack is smaller in cup-cone fracture of a round bar than in slant fracture of a plane strain specimen, and Gurson and Rousselier model differ by the predicted inclination angle of the slant crack

REFERENCES

[1] Gurson, A. L.: *J. Engng. Mater. Technology* 99 (1977), pp. 2-15.
[2] Tvergaard, V.: *Int. J. Fracture* 18 (1982), pp. 237-252.
[3] Tvergaard, V. and Needleman, A.: *Acta metall.* 32 (1984), pp. 157-169.
[4] Needleman, A. and Tvergaard, V.: *J. Mech. Phys. Solids* 32 (1984), pp. 461-490.
[5] Rousselier, G.: *Nuclear Engineering. and Design* 105 (1987), pp. 97-111.
[6] Needleman, A. and Tvergaard, V.: *J. Mech. Phys. Solids* 35 (1987), pp. 151-183.
[7] Sun, D.-Z., Siegele, D., Voss, B. and Schmitt, W.: *Fatigue Fract. Engng. Mater. Struct.* 12 (1988), pp. 201-212.
[8] Brocks, W., Klingbeil, D., Künecke, G., and Sun, D.-Z.: In: *Second Symposium on Constraint Effects*, *ASTM STP* 1224, M. Kirk and A. Bakker (Eds), 1995, pp. 88-99.
[9] Xia, L., Shih, C.F., and Hutchinson, J.: *J. Mech. Phys. Solids* 43 (1995), pp. 389-413.
[10] Becker, R., Needleman, A., Richmond, O., and Tvergaard, V.: *J. Mech. Phys. Solids* 36 (1988), pp. 317-351.
[11] Becker, R. and Needleman, A.: *J. Appl. Mech.* 53 (1986), pp. 491-499.
[12] Leblond, J.-B., Perrin, G., and Devaux, J.: *J. Appl. Mech.* 61 (1994), pp. 236-242.
[13] Rice, J.R.: In: *Proc. 14th Int. Conf. Theoretical and Appl. Mech.*, W. Koiter (Ed), Delft, 1976.
[14] Rudnicki, J. and Rice, J.R.: *J. Mech. Phys. Solids* 23 (1975), pp. 371-394.
[15] Yamamoto, H,: *Int. J. Fracture* 14 (1978).
[16] Tvergaard, V.: *J. Mech. Phys. Solids* 30 (1982), pp. 399-425.
[17] Mear, M. and Hutchinson, J.: *Mechanics of Materials* 4 (1985), pp. 395-407.
[18] Tvergaard, V.: *J. Mech. Phys. Solids* 35 (1987), pp. 43-60.
[19] Doghri, I. and Billardon, R.: *Mechanics of Materials* 19 (1995), pp. 129-149.
[20] Chu, C. and Needleman, A.: *J. Engng. Mater. Technology* 102 (1980), pp. 249-256.

[21] Besson, J., Brocks, W., Chabanet, O., and Steglich, D.: *Europ. J. of Finite Elements* (2001), accepted.
[22] Besson, J., Steglich, D., and Brocks, W.: *Int J. Plasticity*, submitted
[23] Aravas, N.: *Int. J. Num. Meth. Engng*. 24 (1987), pp.1395-1416.
[24] Foerch, R., Besson, J., Cailletaud, G., and Pilvin, P.: *Computer Methods in Applied Mechanics and Engineering* 141 (1997), pp. 355-372.
[25] Besson, J., Steglich, D., and Brocks, W.: *Int J. Solids Structures*, accepted.
[26] Zhang, Z.: *Compt. Methods Appl. Mech. Engrg.* 121 (1995), pp. 15-28.
[27] Hughes, T. and and Winget, J.: *Int. J. Num. Meth. Engng*. 15 (1980), pp.1862-1867.
[28] Rice, J.R. and Rudnicki, J.: *Int J. Solids Structures* 16 (1980), pp. 597-605.
[29] Rivalin, F.: PhD thesis, École des Mines de Paris, 1989.
[30] Steglich, D.: PhD thesis, Technical University of Berlin, 1999.
[31] Ruggieri, C., Panontin, T.L., and Dodds, R.H.: *Int. J. Fracture* 82 (1996), pp. 67-95.
[32] Siegmund, Th. and Brocks, W.: *Int. J. Fracture* 99 (1999), pp. 97-116.
[33] Sun, D.-Z. and Hönig, A.: *Proc. Third Int. Conf. on Localized Damage*, M.H. Aliabadi, A. Carpinteri, S. Kalisky and D. J. Cartwright (Eds), 1994, pp 287-296.
[34] Steglich, D. and Brocks, W.: *Fatigue Fract. Engng. Mater. Struct*. 21 (1998), pp.1175-1188.
[35] Gullerud, A.S., Gao, X., Dodds, R.H., and Haj-Ali, R.: *Engng. Fracture Mechanics* 66 (2000), pp. 65-92.
[36] Brocks, W., Sun, D.Z., and Hönig, A.: *Int. J. Plasticity* 11 (1995), 971-998.